ATLAS Collaboration ATL-COM-MUON-2004-0xx
July 1, 2004

Study of temperature and gas composition effects in rt relations of Atlas MDT BIL Chambers

A.Baroncelli, E.Graziani, S.Tagliaventi

Dipartimento di Fisica "E.Amaldi", Università degli Studi Roma Tre
and INFN, Sezione di Roma III
Via della Vasca Navale, 84 I-00146 Roma

P.Bagnaia, E.Solfaroli

Dipartimento di Fisica, Università degli Studi "La Sapienza"
and INFN, Sezione di Roma
P.le Aldo Moro, 2 I-00185 Roma

ATL-MUON-2004-018
15 July 2004

Abstract

Large samples of cosmic rays taken at the Roma Tre test stand using precisely calibrated gas bottles have been used to study temperature and gas composition effects in spectra and rt relations of MDT BIL chambers of the Atlas experiment. Results are presented in this note. A comparison with Garfield expectations is also shown.

1 Introduction

MDT tubes of BIL chambers will be operated at a gas composition of Ar/CO_2 93/7 and at 3080 V. Space-time rt relations of MDT tubes are expected to depend significantly on gas composition [1]. A change of 1% in the gas composition around the nominal value determines a variation which is expected to be as large as 10% in the maximum drift time. Temperature is also expected to affect the charge collection in MDT tubes via two different mechanisms. The drift velocity increases with temperature and induces an overall shortening of the drift spectrum; at the same time the decrease of the gas density is such that the distance between primary ionization clusters increase and the signal takes a longer time to pass the discriminator threshold, as electrons have to undergo a longer path. This second mechanism is likely to be of some importance for small drift radii only. The understanding of these effects is important not only in itself but also because it may turn out to be possible to store the parameters of the analytical corrections between two rt files that account for temperature and gas composition variations.

This note is organised as follows. Section 2 describes the experimental setup used and the way data were organised and analysed. Section 3 gives a description of the temperature and of the atmospheric pressure measurements. Sections 4 and 5 provide results obtained for drift time spectra and for rt relations at different temperatures and gas compositions. Section 6 discusses about a possible parametrisation of the observed temperature effects and its use in the calibration procedure. Finally, section 7 summarises results and conclusions.

2 Data analysis and samples

A large sample of cosmic muons was taken at the Roma Tre Atlas test site with the MDT BIL chamber RM1020. Data taking began on 26/11/2003 and lasted ten days later. The test site is described in detail in [2] and consists of a cosmic ray hodoscope that reproduces on a smaller scale the MDT configuration in the Atlas muon spectrometer. The hodoscope provides an almost uniform illumination of the BIL chamber surface: it is made of three planes of RPC that provide both a measure of the coordinate along the drift tube and a fast trigger with a resolution of about 1 ns. Six different trigger sectors, in the direction along the drift tube, are defined: they select cosmic ray tracks almost perpendicular to the BIL chamber surface, with an aperture of about 12° around the vertical axis.

The used gas was provided by premixed bottles containing 10^4 l of two precisely determined gas mixtures of Ar/CO_2 93/7 and 93.3/6.7 The CO_2 percentage was known from the manifacturer with a relative precision of 0.5% (0.035% absolute) while the Ar content was complemented to 100%. According to ref. [1] such an uncertainty on the CO_2 percentage can lead to systematic effects of the order of 20 μm on rt relations and of 2.5 ns on the length of the maximum drift spectrum. These values are at least of the same order, if not larger, than the accuracy to be reached in this study. It was thus decided to limit the analysis of the effects of temperature variations only to set of data taken with the same bottle (where one bottle corresponded to one data acquisition run). Cosmic rays data were collected with one MDT BIL chamber fluxed with 200 l/h for a period of about

5 days at each of the two gas mixtures. Due to the uncertainty on the bottle-to-bottle gas composition, the first part of the statistics for each run, corresponding to one full gas chamber volume exchange, was discarded: this amounted to about 1/6 of the statistics for each run.

A total sample of 6M of events was collected for each gas composition.

The test site cosmic ray experimental set-up is very different under many respects from the H8 test beam set-up. During test beam operations, usually very fast runs, with a reasonably constant temperature, scan a very small amount of drift tubes. From this point of view, the Roma Tre experimental set-up is more similar to the real conditions that the Atlas experiment will meet in the LHC cavern.

The auto-calibration package CALIB [3] has been used in the present analysis. The analysis procedure is shortly described in the following. The first step consists in time equalisation of different tubes for the six different trigger sectors: this accounts for possible differences in electronic channels. Then, for each tube, the drift time distribution was parametrized and fitted with an empirical 8 parameter function. A typical drift spectrum is shown in fig. 1, where the two insets magnify the region of the minimum and maximum drift time (called t_0 and t_1 in the following, with $t_{max} = t_1 - t_0$). The start and end point of the distribution are typically determined with a precision of 0.5 and 1 ns respectively. The end point of the drift time distribution was fitted for each temperature sample separately (see below). The start point t_0 is expected to have a very weak dependance upon the temperature. Changes in t_0 are caused by gas gain variations with the temperature, which, accordingly to the Diethorn formula [1] and for the geometry of the MDT tubes, are proportional to about $10 \times \Delta T$. Assuming a linear signal rising edge and a 20 electron threshold, this yields a shift of the threshold crossing time of the order of $-0.1\ ns/K$. The spectrum start point t_0 was thus fitted on the full sample, in order to minimise the statistical error (see also sec. 6) which dominates. The second step of the analysis consists in iteratively computing the rt relation. Each multilayer is treated separately. The average residual after the last iteration as a function of the drift radius is always much less than 1 μm for all processed samples at all distances. No constraints are imposed on the rt determination: rt values saturate at about 600 μm in the wire region, a number which is compatible with the time of arrival of the last electron which allow the signal to pass the threshold. Hits for the rt determination are accepted in a time window which starts 16 ns before t_0 (see fig. 1) and has no upper limit. The final rt relation is stored as a 110 entries table. An alternative representation can be obtained by fitting the data points with a Chebychev polinomial of 12-th order, for which the storage of the fitted coefficients only is needed. A typical rt relation obtained with the described procedure is shown in fig. 2: also shown is the analytical representation with 12-th order Chebychev polynomial. Figure 3 shows in the inset an example of the difference between the data points and the fit: the same distribution is shown as a function of the drift time in the main part of the figure.

All muon hits of all events were assigned a temperature computed using the different temperature probes, with a model described in detail in the next section. All hits were grouped in bins of limited temperature interval and analysed separately. Data were processed selecting hits collected in a given temperature range and the corresponding space time relation was assumed to be the space time relation of that gas composition at the

average temperature of the selected temperature window. Temperature and composition effects on the space time relations are defined in the present note as the difference between two different rt relations, $\delta r_{\Delta T,\Delta C}$, obtained in different conditions.

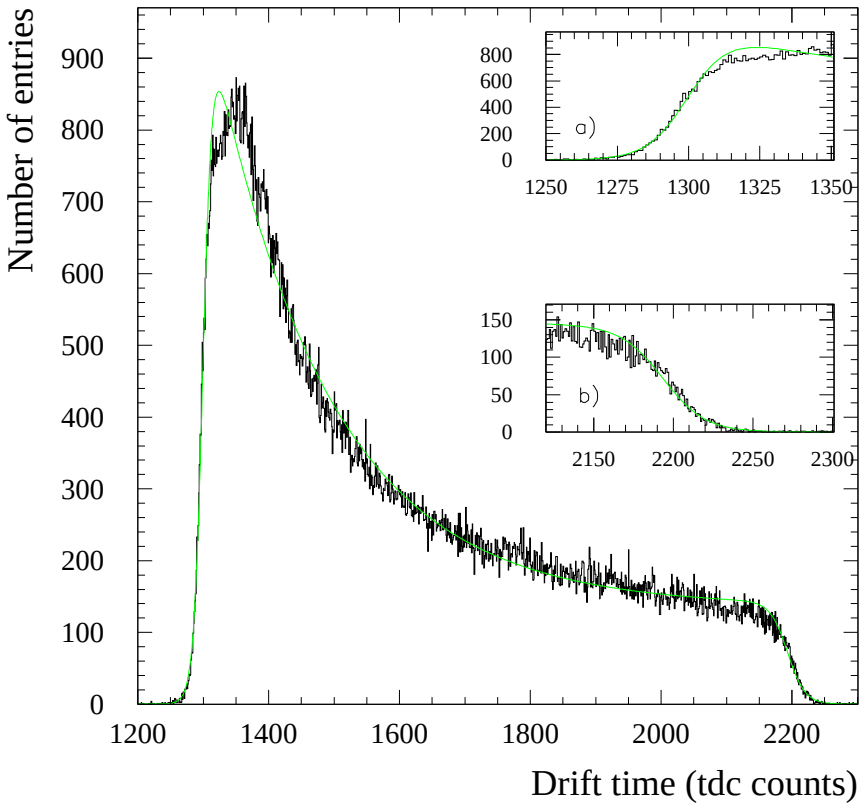

Figure 1: Drift time distribution. The light (green) line superimposed on the histogram is the result of the 8 parameter fit procedure described in the text. The two insets show a magnified view of the mimimum and maximum drift time regions.

3 Temperature and atmospheric pressure measurements

Eight LM35 National Semiconductor temperature probes were placed on the two multilayers of the MDT chamber: five on the upper one and three on the lower one. The probes were first inter-calibrated to avoid possible measurement bias: their resolution was measured to be about 0.1 ^{o}C. During data taking, temperatures were recorded every 10 seconds and averaged values over an interval of eight minutes were used in the analysis. The top panel of figure 4 shows the room temperature as a function of data taking time, as measured by a probe placed in the centre of the upper multilayer. Typical day-night

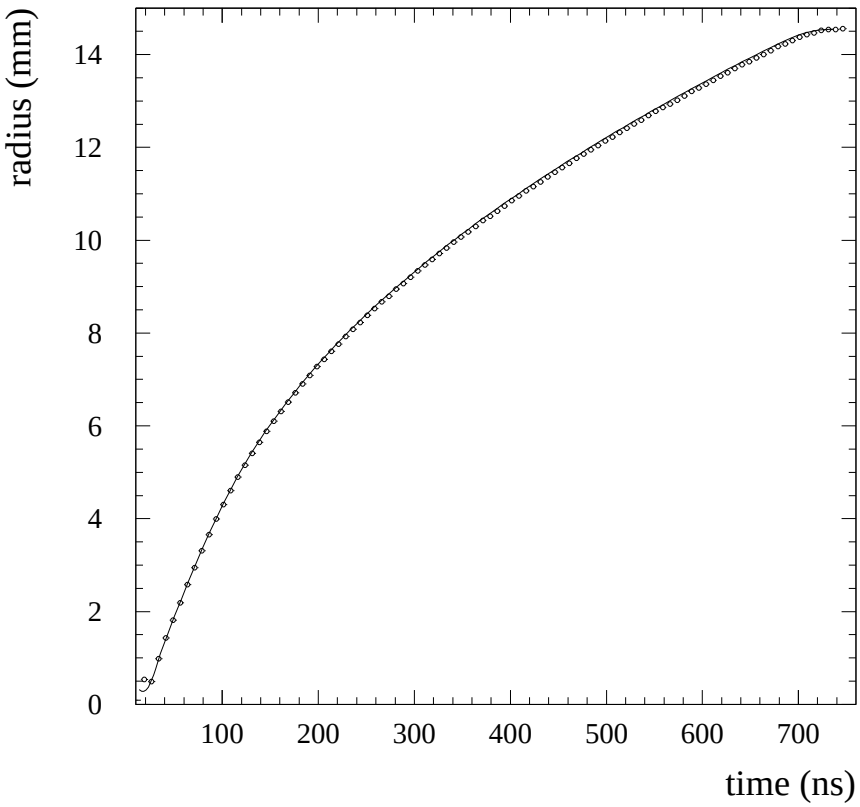

Figure 2: Typical rt relation for one MDT BIL tube as determined by the iterative procedure described in the text. Superimposed function describes the fit of data points with a 12-th order Chebychev polynomial.

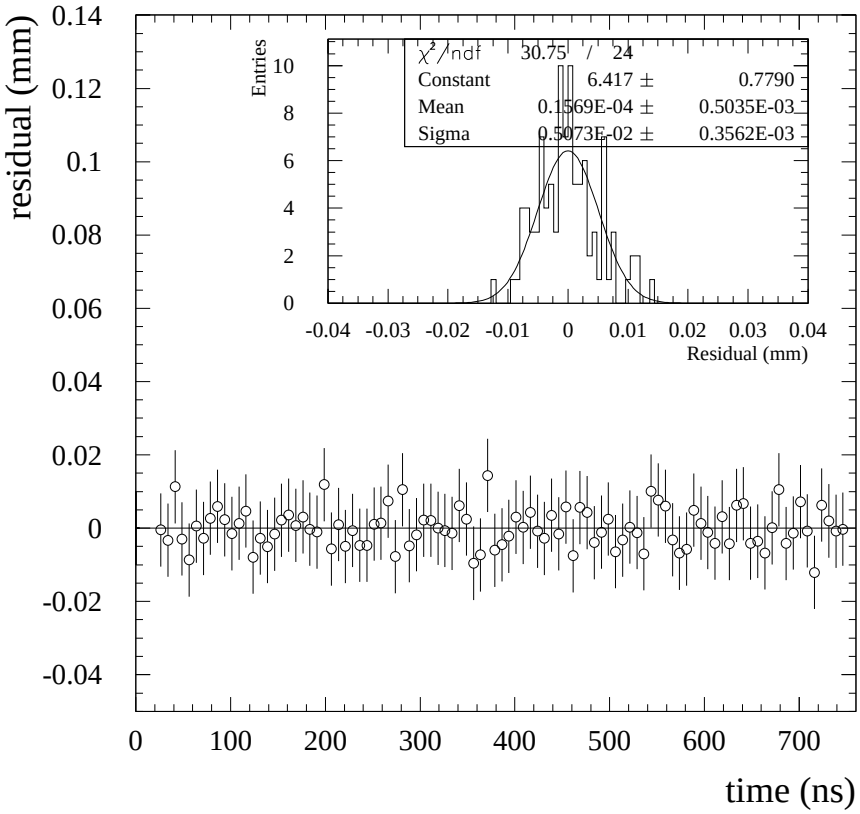

Figure 3: Fit residuals of rt relation for one MDT BIL tube as determined by the iterative procedure described in the text. The main part of the figure shows the distribution as a function of the drift time; the inset shows the projection along the ordinate axis.

cycles are easily recognized. In order to enlarge temperature excursions in those winter days, the air conditioning system was used during some of the nights.

Temperature gradients along the directions parallel (longitudinal) and perpendicular (transverse) to the MDT tubes were studied. Longitudinal temperature gradients are expected to be more important due to the presence of the readout electronics on one side of the multilayers, which acts as a heat source. The bottom panel of figure 4 shows the temperature gradients, as a function of the data taking time, measured between the two sides of the upper multilayer and between the centre of the same multilayer and its left hand side. As expected, temperature variations along the transverse direction are much smaller and were neglected in the analysis. Longitudinal temperature gradients are of the order of 1 ^{o}C and also follow room temperature cycles.

A simple interpolation model was developed to estimate the temperature in a generic point along the longitudinal direction: this was based on the probe measurements on the two sides of the multilayer and on the assumption of an exponential decay of the temperature as a function of the distance of the point from the side which houses the readout electronics. The free parameter of the model (the exponential attenuation length) was evaluated by comparing predicted temperatures with measured ones, in points where additional probes were present. Residual temperatures were then used to validate the model and to estimate the measurement resolution: this is shown in figure 5, where the difference between the predicted and the measured temperature at the centre of the upper multilayer is plotted as a function of the data taking time. A resolution of about 0.1 ^{0}C was estimated, largely sufficient for the needs of this analysis. Systematic effects, which are visible in the plot, also lie in the same range and are of no worry. After this procedure was applied, each muon hit was assigned a temperature, then used in the analysis.

Further checks on the thermal properties of the MDT BIL chambers were performed after the data taking was over. As the temperature probes were all placed on the upper surface of the two multilayers, one could in principle think of possible temperature gradients in the vertical direction, leading to different temperatures on different tube layers. Tubes are thermally isolated one from each other by the glue which keeps them together. Possible delays in temperature variations of internal tube layers at variations of external temperature might have had some effects. This was checked by placing additional temperature probes in the interstitial spaces between the internal tube layers, in central position along the tube direction. Temperature measurements were then repeated in conditions very similar to those of the data taking. Fig. 6 shows in the top panel the difference between the temperature measured on the multilayer surface and in the innermost position (between the second and third tube layer), and in the bottom panel the room temperature. Delays of the order of one hour and more are clearly discernible around the turning points of the room temperature: overall effects are anyway at the level of 0.1-0.2 $^\circ C$ and can be safely neglected.

The gas distribution system in use at the Roma Tre test site sets the gas pressure using the atmospheric pressure as reference. It is then important to monitor the time variations of the atmospheric pressure. Figure 7 shows the atmospheric pressure as a function of the data taking time. Pressure effects are expected to be less important than temperature ones. According to the ideal gas equation, the change in gas density induced by a variation of 1^oC at room temperature is equivalent to a pressure variation of

$-3000/300\ mbar = 10\ mbar$ at a pressure of 3000 $mbar$. In order to take into account atmospheric pressure variations during the data taking, an effective temperature was thus introduced: an additional term $-\Delta p/10\ ^{\circ}C$ was added to the previously described estimated temperature, where Δp is the difference between the current and the reference pressure (which was fixed to the one measured at the beginning of the data taking). All the analyses in the following use this effective temperature.

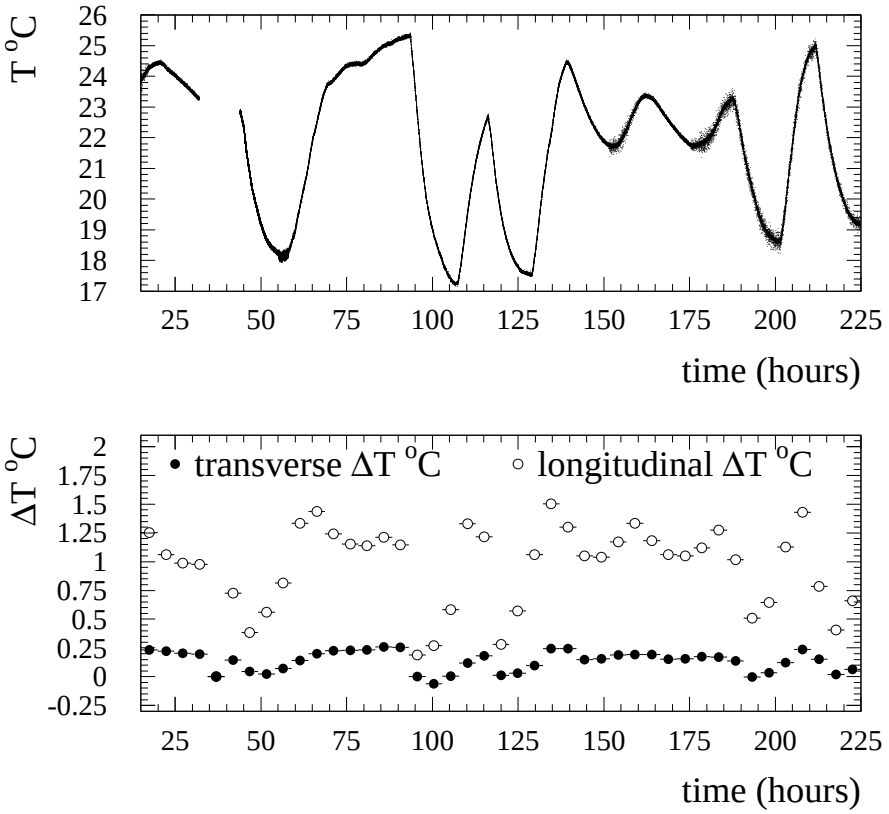

Figure 4: Top panel: room temperature as a function of time, measured at the centre of the upper multilayer. Bottom panel: longitudinal and transverse temperature gradient as a function of time, measured between the two sides of the upper multilayer and between the centre of the upper multilayer and its left hand side respectively.

The temperature distribution of all the hits in one run and for one multilayer is shown in figure 8. It extends between about 15.5 and 22 degrees centigrade. Also shown are the four temperature intervals used in the analysis for that run. They were chosen so as to have an approximately equipopulation in each interval.

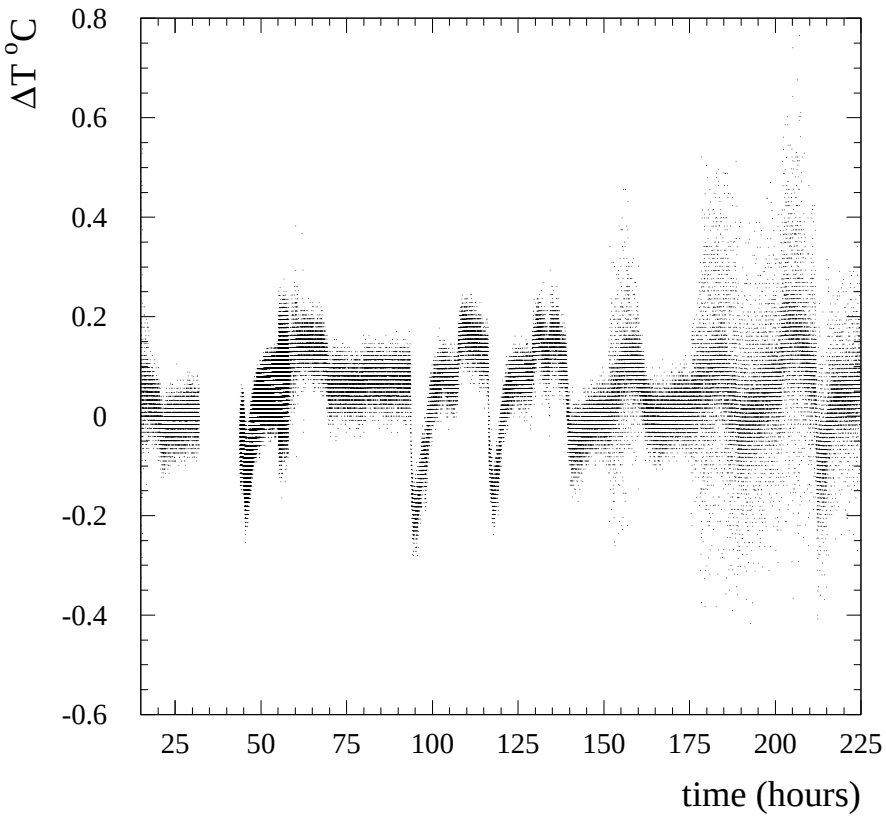

Figure 5: Difference between the predicted and measured temperatures at the upper multilayer centre as a function of data taking time.

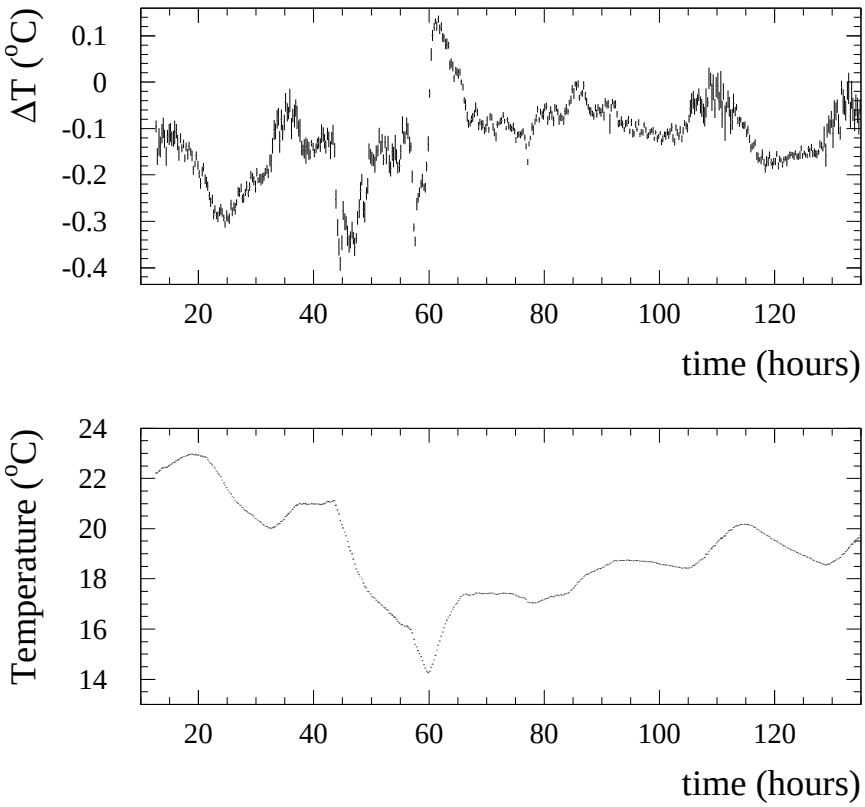

Figure 6: Top panel: difference between room temperature and the temperature measured between the second and third tube layer, in the upper multilayer. Bottom panel: room temperature.

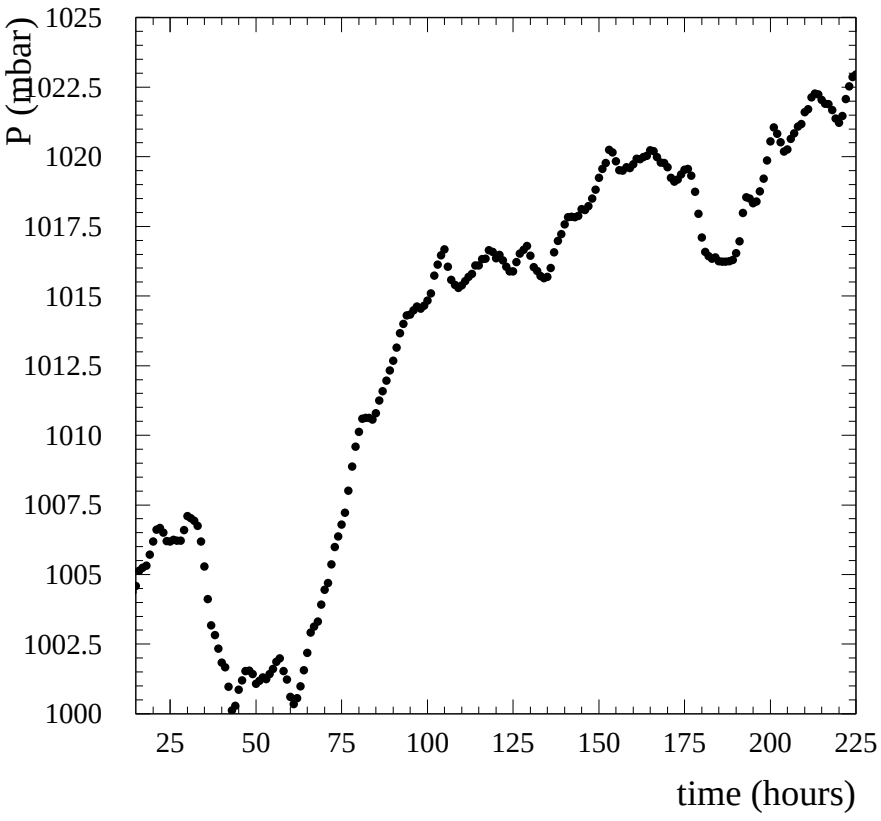

Figure 7: Atmospheric pressure as a function of data taking time.

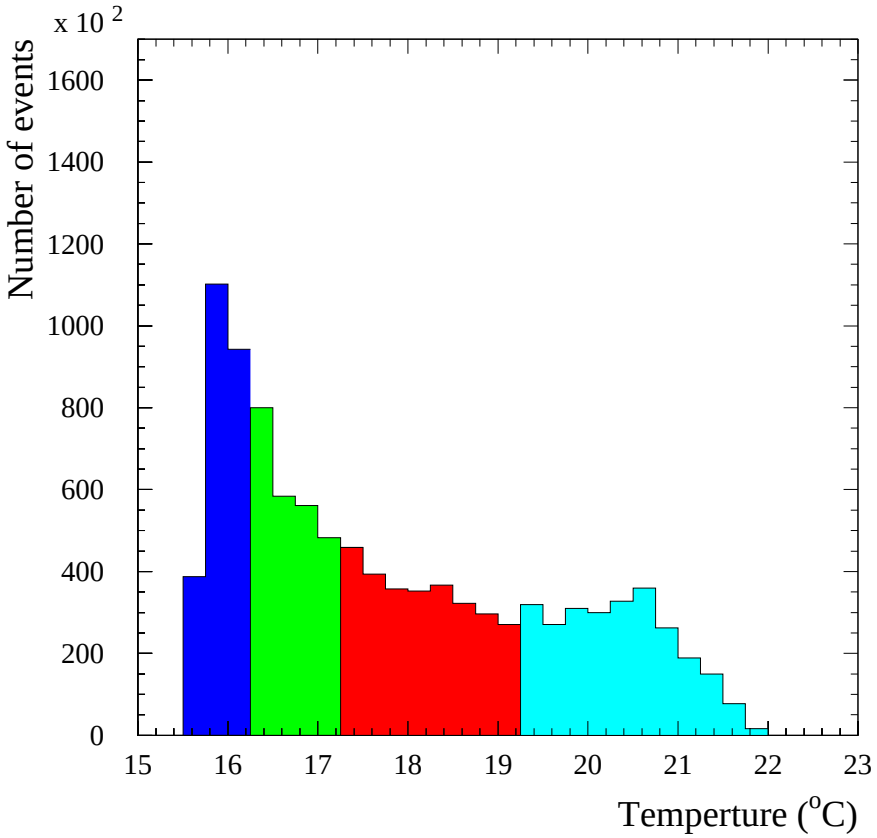

Figure 8: Temperature distribution of the hits used in one run in the present analysis. Temperature intervals, shown in different colours, were chosen so as to have an approximately equipopulation in each interval.

4 Results: drift time spectra

The maximum drift time t_{max} was fitted for each run and for each multilayer separately in different temperature interval. Figure 9 shows, as an example, the results obtained for the upper multilayer for three different runs at the nominal gas composition Ar/CO_2 93/7. As expected, the maximum drift time length decreases with increasing temperature due to the dominant effect of the decrease of the gas density, which in turn causes an increase in drift velocity. Also shown in fig. 9 are the results of linear fits on data points for each run separately. While the absolute maximum drift time length fluctuate from run to run due to the uncertainty on gas composition provided by the single bottles, the slopes are quite compatible each other (see also fig. 10). Extrapolating the three fitted functions in fig. 9 at 21 $^{\circ}C$ resulted in an rms spread of about 3 ns, to be compared with the 2.5 ns expected from the known uncertainty on gas composition provided by the manifacturer and from the calculations in ref. [1]. Fitted slopes for the full statistics, including also runs taken with the nominal gas composition Ar/CO_2 93.3/6.7 and for each multilayer separately are shown in fig. 10. The average result for the temperature effect on maximum drift time length is $-2.34 \pm 0.06\ ns/K$. This result is in good agreement with an analogous result obtained at the H8 beam test setup ([4]), in quite different experimental conditions, and in marginal agreement with the expectations of the Garfield simulation program [5], which predicts a value of $-2.6\ ns/K$.

5 Results: rt relations

In the following $rt_{T,C}(t)$ indicates the space time relation as determined at a temperature T and composition C; it gives the drift radius as a function of the drift time t. The difference between two space time relations, corresponding to temperature and composition T_1, C_1 and T_2, C_2 respectively will be indicated as

$$\delta_{rt} = \delta r_{\Delta T, \Delta C}(t) = rt_{T_1,C_1}(t) - rt_{T_2,C_2}(t)$$

where $\Delta T = T_1 - T_2$ and $\Delta C = C_1 - C_2$.

A first set of results concerns the difference between two rt relations obtained using the same gas composition at different temperatures. A second set concerns the difference between two rt relations, $\delta r_{\Delta T,\Delta C}$, obtained at different gas compositions and temperatures. These results are described in the two following sections.

5.1 Temperature effects

Figures 11 and 12 show the variation of the rt relation, $\delta r_{\Delta T,\Delta C}$, obtained at a gas composition of 93/7 Ar/CO_2 corresponding to different temperature jumps as observed in multilayer up and down respectively. The $\delta r_{\Delta T,0}$ of two different multilayers are observed to be approximately the same for close temperature jumps. The pattern of δ_{rt} as a function of time is approximately the same for all temperature jumps: it goes below zero, where it reaches a minimum around 100 nsec, it crosses zero around 200 nsec and

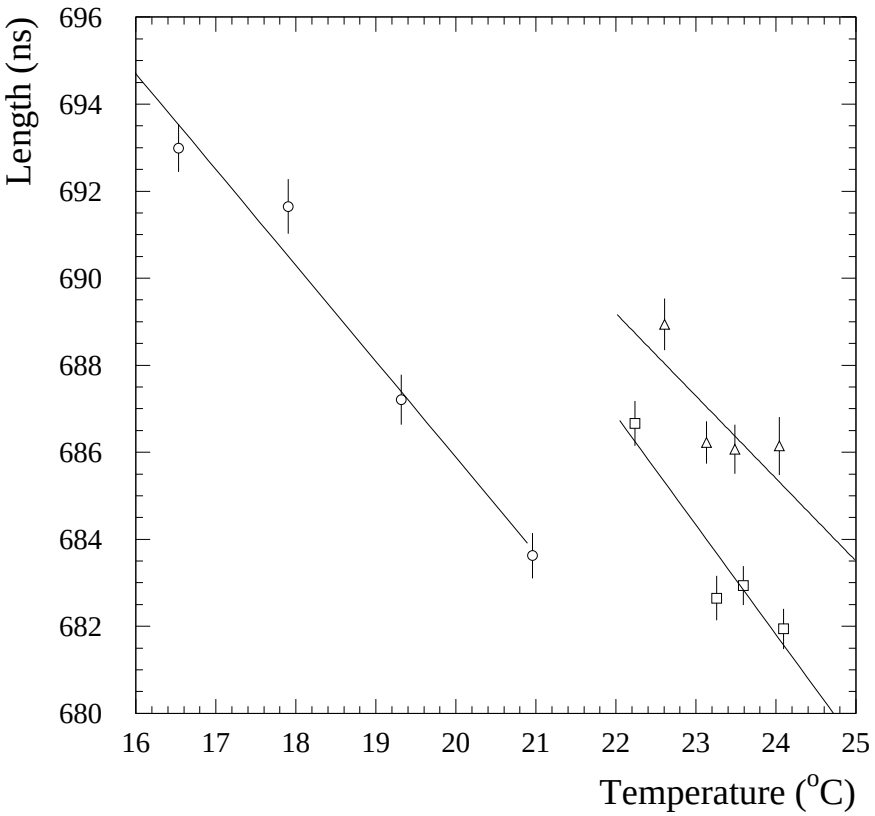

Figure 9: Maximum drift time lengths for three different runs as a function of the temperature (upper multilayer only). Also shown are linear fit results for the three runs separately.

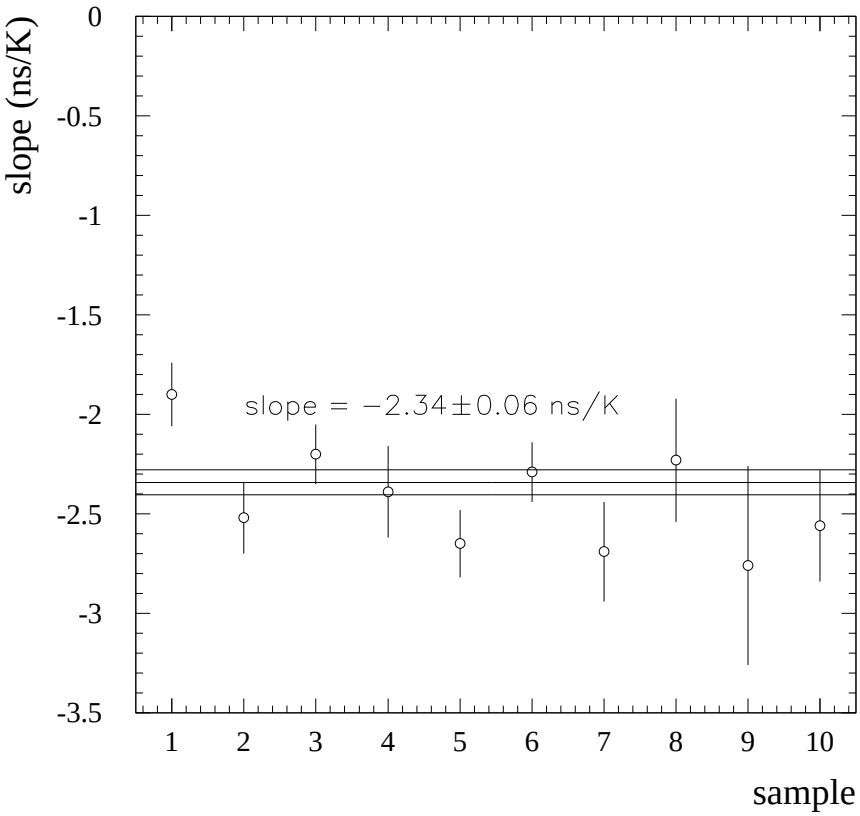

Figure 10: Fitted slopes of maximum drift time length vs temperature for the full available statistics.

then slowly increases to the maximum value up to the end of the drift time spectrum. Both minimum (maximum) values of δ_{rt} decrease (increase) approximately linearly with temperature jumps.

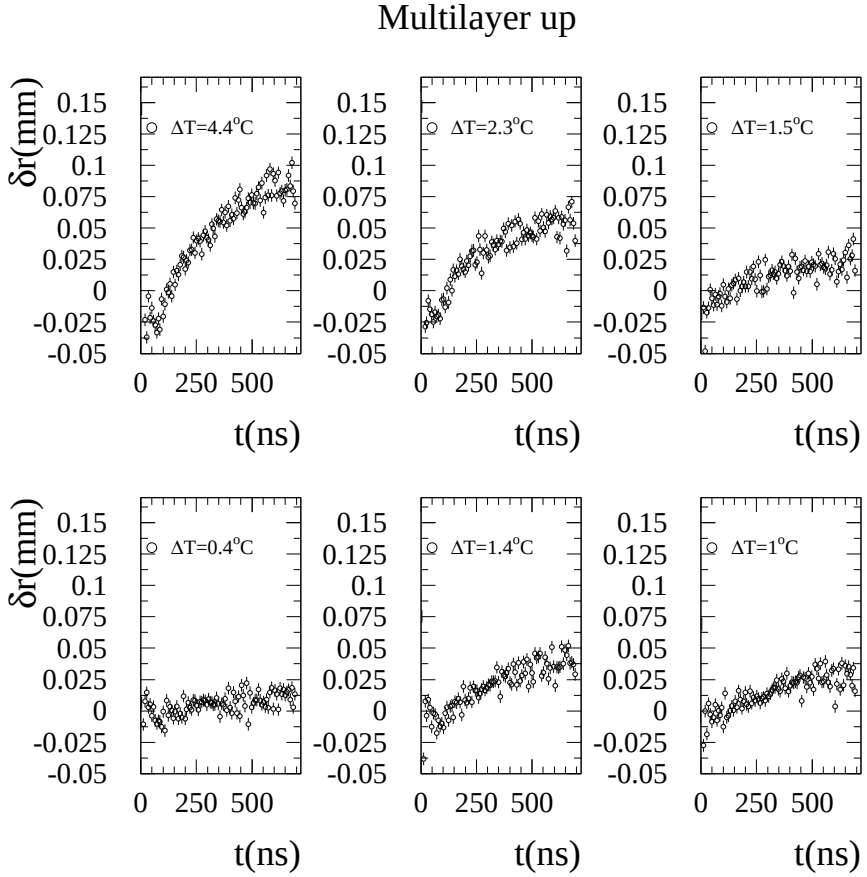

Figure 11: $\delta r_{\Delta T,\Delta C}$ as a function of time and for various temperature jumps as measured in upper multilayer

5.2 Composition effects

Composition and temperature effects are expected to affect simultaneously the rt relations. Figure 13 shows $\delta r_{\Delta T,\Delta C}$ for different values of ΔT when the difference between the two rt relations is measured using the two different gas compositions of Ar/CO_2 93/7 and 93.3/6.7. As expected, composition effects are sizeable and as large as > 200 μm for large drift times. The family of points which corresponds to the lowest value of ΔT is expected to be mostly the effect of change of gas composition. For this reason, the family of points of figure 13 which corresponds to ΔT=0.3^{o}C was subtracted from the families which correspond to higher temperature jumps. If temperature and gas composition effects add up separately, the derived δ_{rt} should thus contain temperature effects only. This is shown in fig. 14 where the difference $\delta r_{\Delta T,\Delta C} - \delta r_{0.3,\Delta C}$

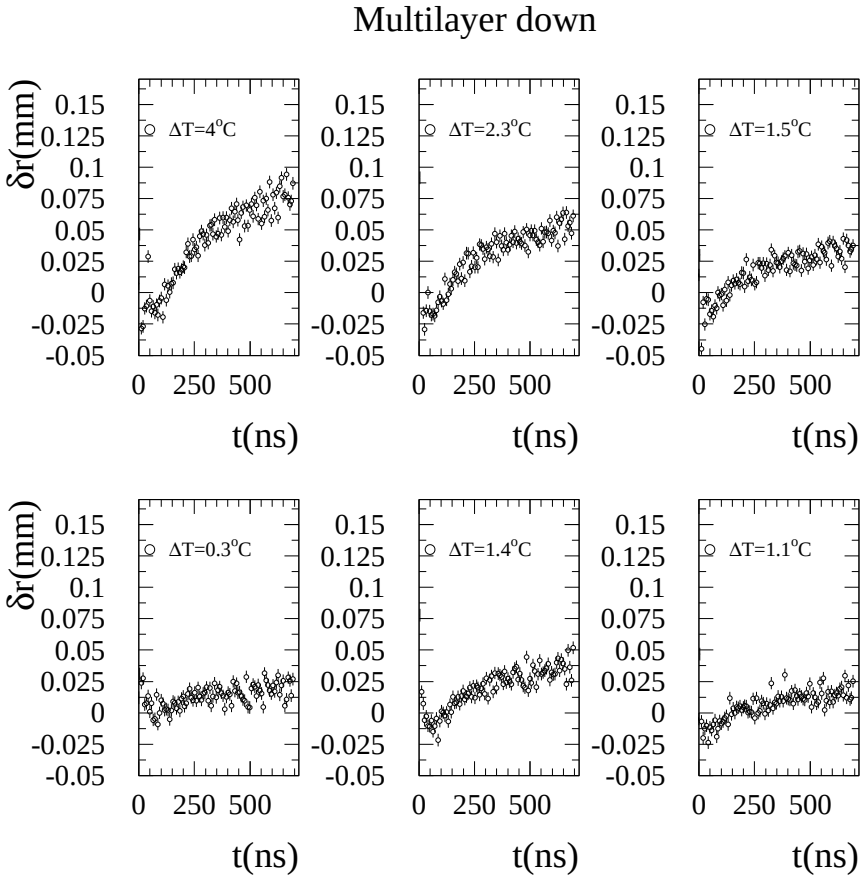

Figure 12: $\delta r_{\Delta T,\Delta C}$ as a function of time and for various temperature jumps as measured in bottom multilayer

is shown as a function of time and for various temperature jumps ΔT. The four families shown in figure 14 are very close to the corresponding families of fig. 11 and 12 which contain temperature effects only. Temperature and composition effects are indeed observed to cumulate as expected:

$$\delta r_{\Delta T,\Delta C} = \delta r_{0,\Delta C} + \delta r_{\Delta T,0}$$

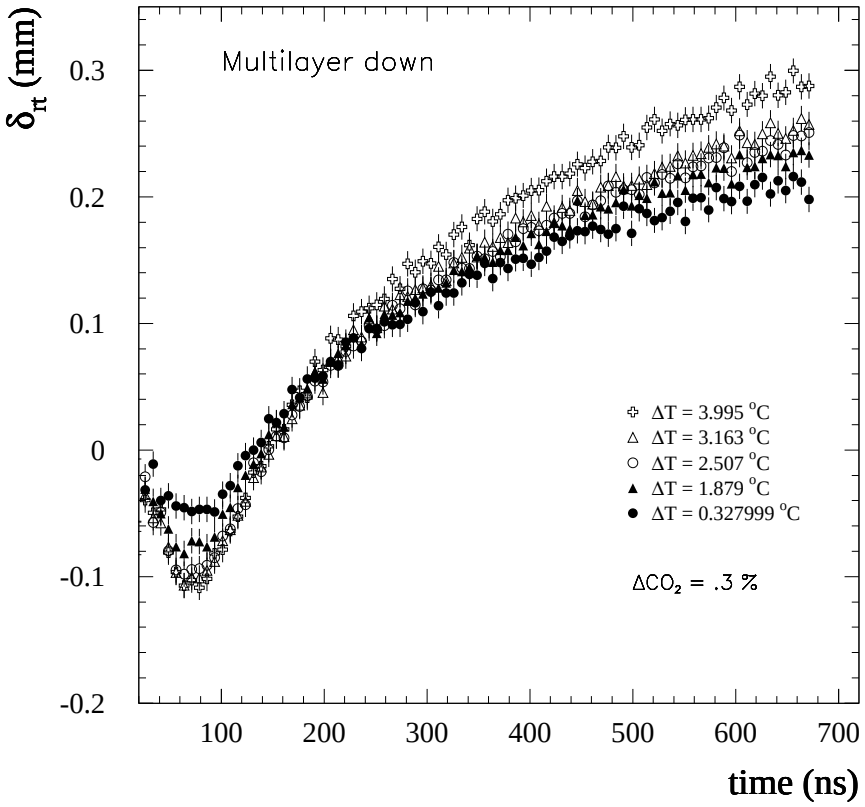

Figure 13: $\delta r_{\Delta T,\Delta C}$ as a function of time and for various temperature jumps for a CO_2variation of .3%. Data from RM3.

5.3 Comparison with Garfield

The response of the detector can be analysed using a full simulation of the MDT and its electronics. Garfield (currently version 7.04) [5] uses the program Heed to reproduce the ionization of the gas molecules by the muons which cross the tubes, and has an interface to the program Magboltz to compute the electron transport properties in the gas. Therefore it simulates the electron and ion drift in the gas, the avalanche, the signal creation and detection, and the transfer function of the electronics. For each muon the program records the time measured by the TDC and the amplitude of the charge, as

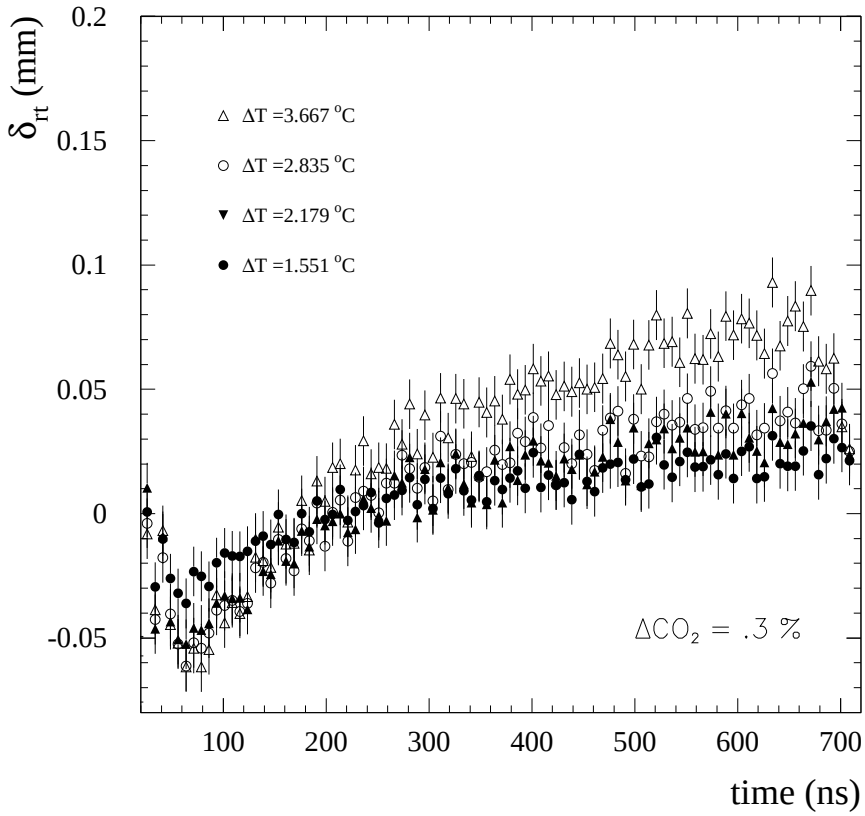

Figure 14: The difference $\delta r_{\Delta T,\Delta C} - \delta r_{0.3,\Delta C}$ is shown as a function of time and for various temperature jumps. Data from RM3.

measured by the Wilkinson ADC. For this study, only the time of the threshold crossing (the "leading edge") has been used in the analysis.

This simulation, which accounts for the fluctuations of the ionization, diffusion and electronics, allows to study the detector response as a function of the gas properties. Many samples of data were generated, with different conditions of some gas parameters, like temperature and composition.

The value of the difference of $\delta r_{\Delta T,\Delta C=0}$ at two fixed drift times of t_2=640 ns and t_1=140 ns (corresponding to approximately the zero crossing point of $\delta r_{\Delta T,\Delta C}$) is shown in figure 15 as a function of the temperature jump. The dependence is approximately linear and corresponds to

$\delta r_{\Delta T,\Delta C}(\Delta t = 500ns) \approx 0.023$*$\Delta$T (mm/^{o}C) = 23 $\mu m/^o$C.

Garfield expectations are also shown in the plot. Although the dependence of the difference of $\delta r_{\Delta T,\Delta C=0}$ at two fixed drift times of t_2=640 ns and t_1=140 ns on temperature jump is linear in both cases Garfield shows a slope which is about 30 % higher.

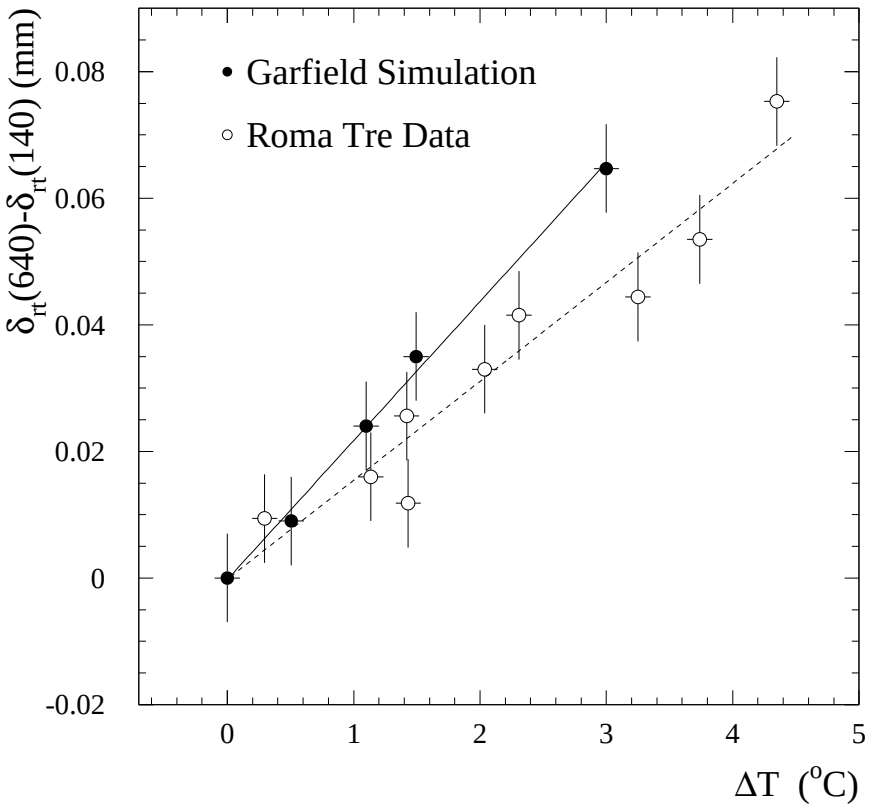

Figure 15: Increase of $\delta r_{\Delta T,\Delta C}$ at a time difference Δt = 500 ns from the minimum as a function of temperature jump. Data from RM3. Superimposed lines are the results of linear fits over the data (dashed) and the Garfield simulation points.

Figures 16 and 17 show a comparison between RM3 data and Garfield data for the two multilayers separately. Each of the six windows per multilayer shows the $\delta r_{\Delta T,\Delta C}$ as observed at a given temperature jump using RM3 data and Garfield data. A good agreement can be observed.

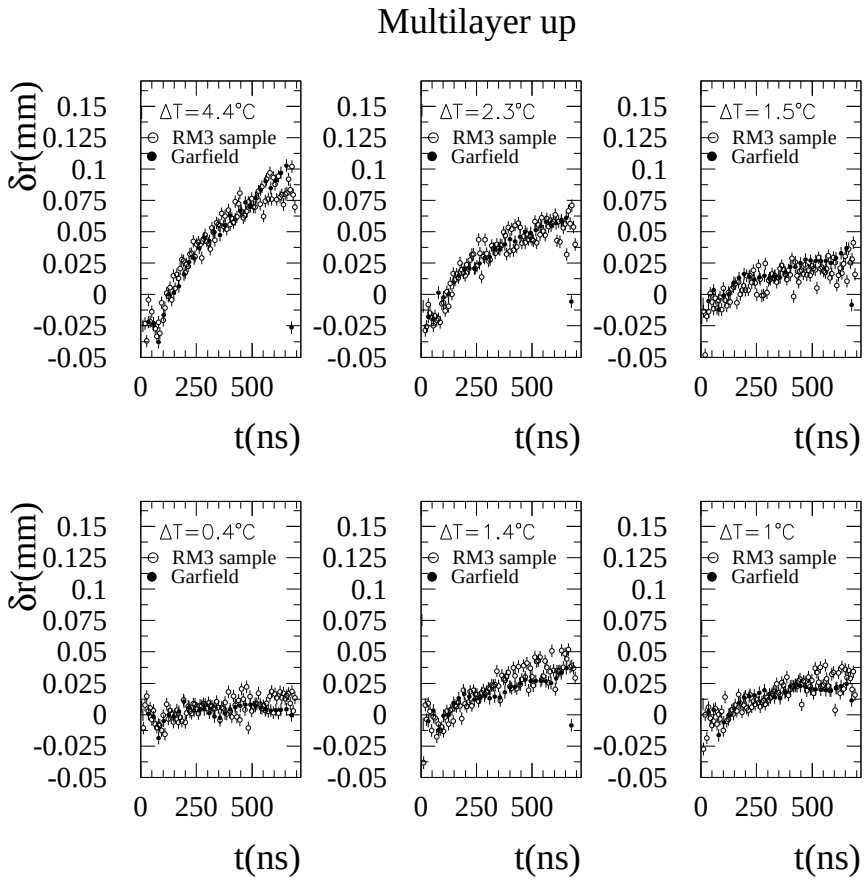

Figure 16: $\delta r_{\Delta T,\Delta C}$ as a function of drift time and for various temperature jumps, as measured in multilayer up. Open circles indicate RM3 data, black points Garfield data.

6 Parameterisations of temperature effects on rt relations

A parameterization of the observed temperature effects has been studied. This may be important for many practical reasons. First of all, the storage volume of rt relations data may be significantly reduced if rt relations are measured at fixed conditions and then evolved between two successive references by accounting for temperature variations, using simple analytic parameterizations. Second, it may be necessary to integrate calibration data over long time intervals, with possibly significant temperature variations. Finally, in some cases, calibration data may be not available and rt relations determined at different conditions may have to be used after correction. If a reference rt relation $rt(t)_{T_0}$ at a

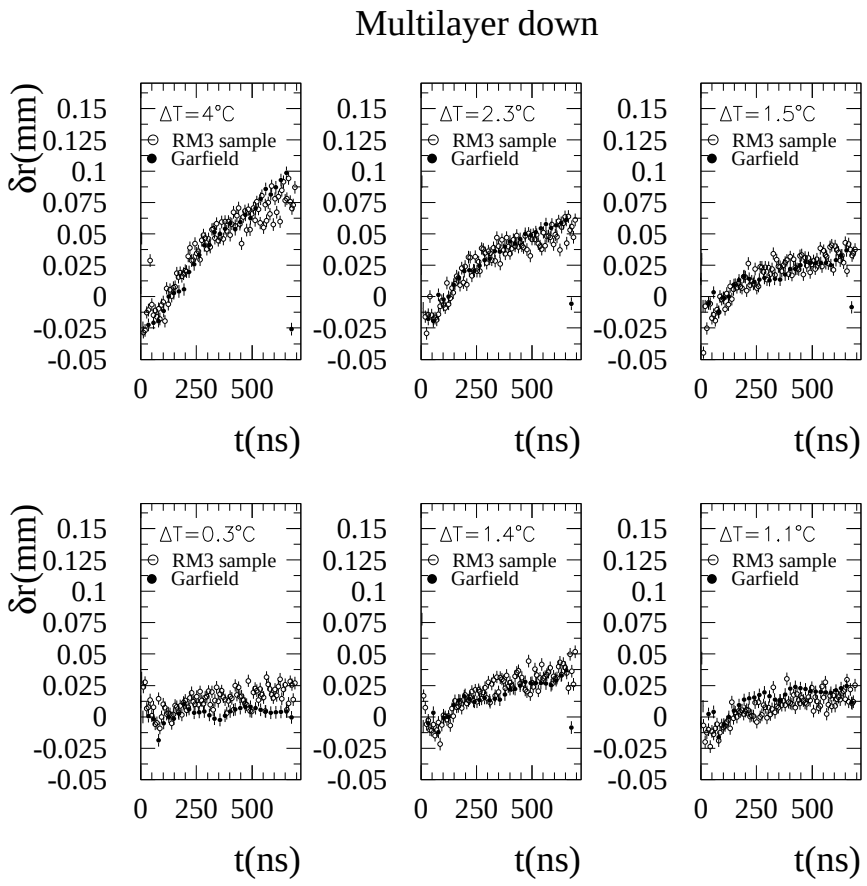

Figure 17: $\delta r_{\Delta T,\Delta C}$ as a function of drift time and for various temperature jumps, as measured in multilayer down. Open circles indicate RM3 data, black points Garfield data.

temperature T_0 is available, then an rt relation at a different temperature T_1 can be computed using the following expression, as suggested by [1]

$$rt_{T,C}(t) = rt_{T_0,C}(t) + (\frac{\rho_0}{\rho} - 1)\left[rt_{T_0,C}(t) - t * rt'_{T_0,C}(t)\right] \quad (1)$$

where ρ_0 and ρ are the gas densities at temperatures T_0 and T respectively: $\frac{\rho_0}{\rho} = \frac{T}{T_0}$ after correcting for atmospheric pressure variations, when necessary. In expression 1 the term $rt'_{T_0,C}(t)$ represents the drift velocity as a function of time at temperature T_0 and was parametrised by making use of the analitical derivative of the corresponding rt relation represented by a 12-th order Chebychev polinomial (see sec. 2). Expression 1 was fitted on the data for each temperature jump, using $\frac{\rho_0}{\rho} = \frac{T}{T_0} = 1 + \frac{\Delta T}{T_0}$, as the only free parameter.

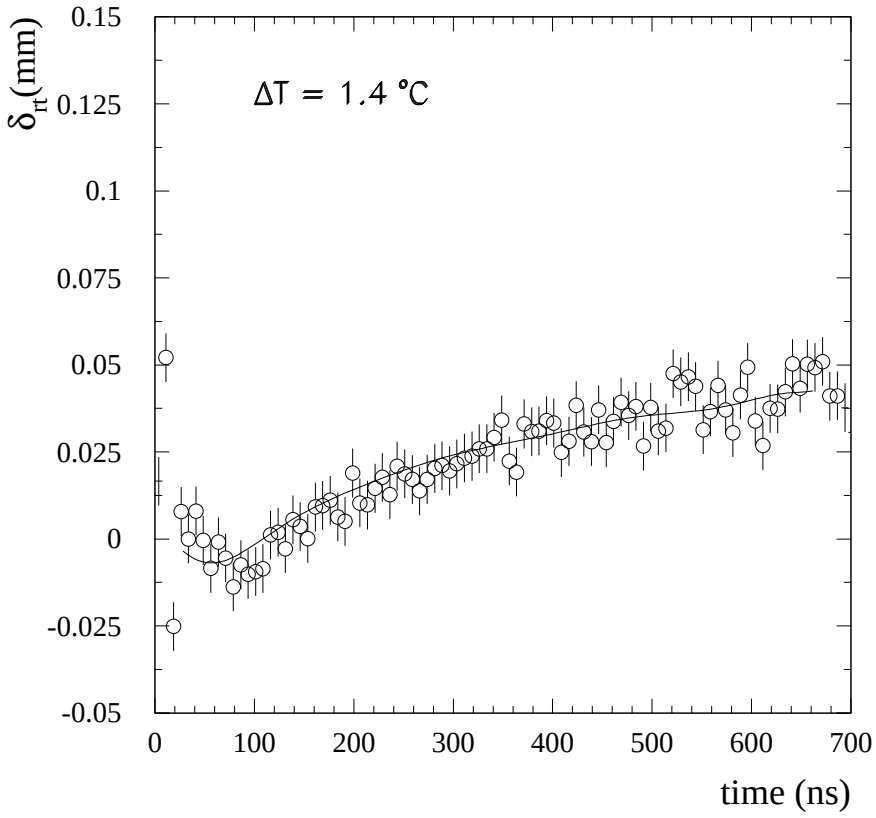

Figure 18: $\delta r_{\Delta T,\Delta C=0}$ as a function of drift time and for a temperature jump of ΔT=1.4^{o}C, in multilayer up. The continuous line indicates the result of the fit described in the text.

Figures 18 and 19 show the result of the fit procedure for ΔT=1.4^{o}C and 4.3^{o}C respectively.

Finally, figure 20 shows a comparison between measured values $(\frac{T}{T_0})_{measured}$ (from temperature and pressure measurements) and fitted values $(\frac{T}{T_0})_{fitted}$. From eq. 1 one expects a linear relation between the two quantities with slope 1 and intercept at (1,1). A linear

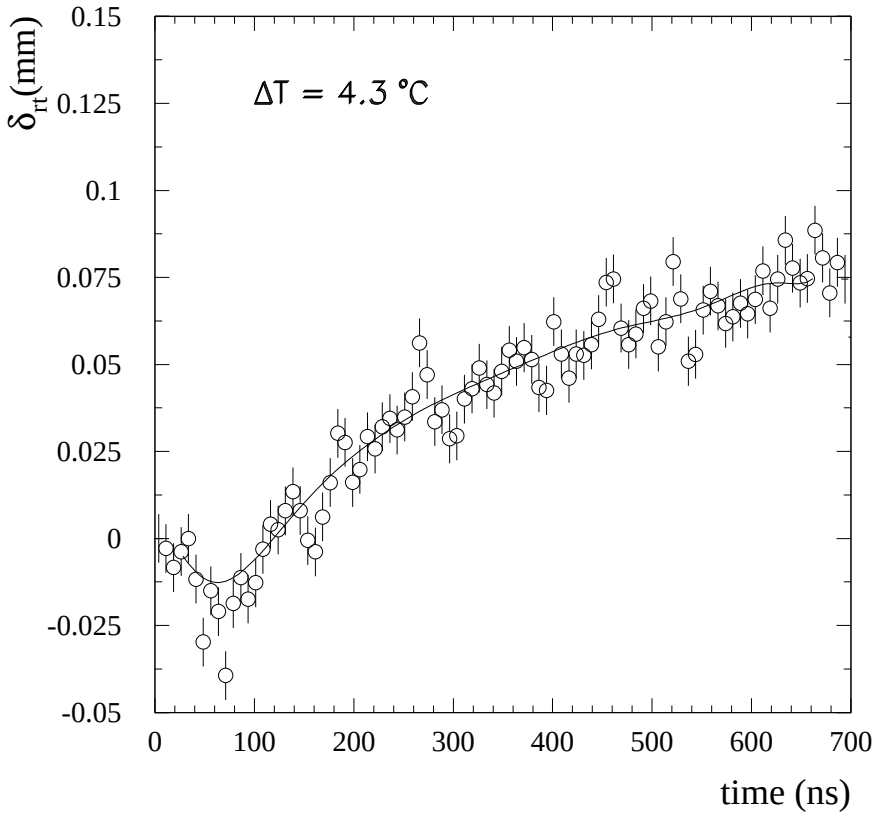

Figure 19: $\delta r_{\Delta T,\Delta C=0}$ as a function of drift time and for a temperature jump of ΔT=4.3^{o}C, in multilayer up. The continuous line indicates the result of the fit described in the text.

fit procedure, with the slope as the only free parameter, gave the result 0.75 ± 0.02, where the error is statistical only. From fig. 20 a remarkably linear relation can be observed. A similar analysis performed on data taken at the H8 test beam setup gave very similar results, which will be presented soon in a dedicated note.

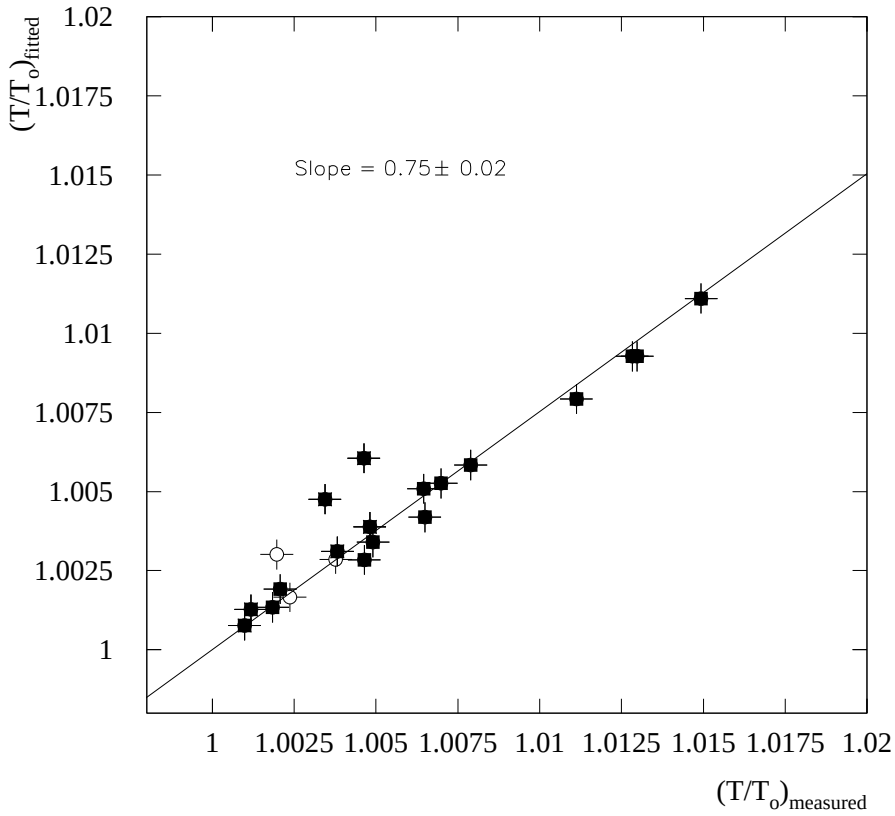

Figure 20: Comparison between measured and fitted values of $\frac{T}{T_0}$. Superimposed is the result of the linear fit with the slope as the only free parameter.

In order to get an idea of the order of magnitude of possible systematics effects on the rt evaluation, the formula in eq. 1 was modified by adding a constant term, to be determined by the fit procedure for each temperature jump. This gave a slope of 1.03 ± 0.02 in the $(\frac{T}{T_0})_{fitted}$ vs $(\frac{T}{T_0})_{measured}$ relation and an estimate for the constant term of 10 μm with a spread of $8\mu m$. Such a systematic effect represents an uncertainty on the rt relation due to a possible rigid shift over all the drift time, which is probably not realistic and has to be regarded just as an estimate of the order of magnitude. A more physical systematic effect could be due to the determination of the start time of the drift time distribution, t_0. A bias in t_0 would cause effects on the rt relation proportional to the drift velocity and thus particularly sizeable for small drift times, where the velocity is large and the radius is small. The minimum drift time, t_0, is expected to depend upon the temperature due to the gain change with the temperature, which affects the threshold crossing time. A rough estimate, with a 15 electron threshold, can be quoted at -0.1 ns/K (see also sec. 2).

In order to evaluate systematic uncertainties on rt determination due to this effect, the formula in eq. 1 was modified by adding a term proportional to the drift velocity:

$$rt_{T,C}(t) = rt_{T_0,C}(t) + (\frac{\rho_0}{\rho} - 1)\left[rt_{T_0,C}(t) - t * rt'_{T_0,C}(t) + c * rt'_{T_0,C}(t)\right] \quad (2)$$

with the parameter c being fitted for each temperature jump.

This gave almost no change in the $(\frac{T}{T_0})_{fitted}$ vs $(\frac{T}{T_0})_{measured}$ relation, as expected, but substantially improved the quality of the individual fits with respect to eq. 1, especially in the small radii region. The mean value for c, averaged over all the temperature jumps, was 0.2 ns/K, which has the opposite sign with respect to what is expected from the gain effect, showing the presence of other systematics at this level.

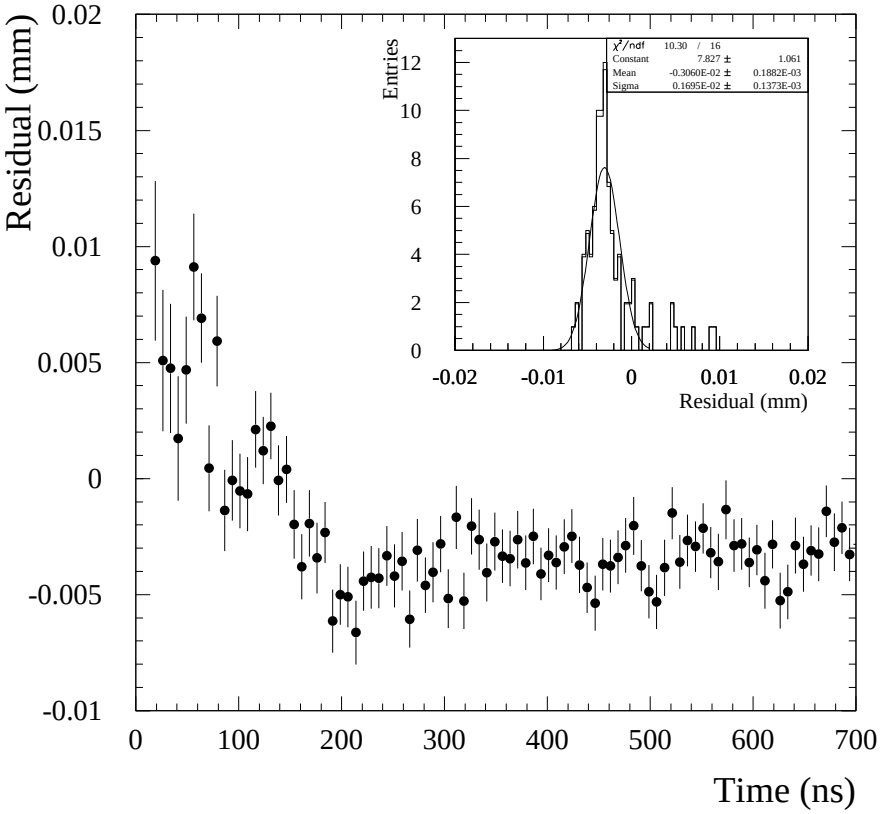

Figure 21: Residuals after CALIB first iteration. Here the starting rt relation is obtained from a relation at a different temperature and then evolved analytically through a corrected form of 1.

The two modified versions of eq. 1 have no predictive power, as they use two more parameters which have to be fitted temperature by temperature. It was thus checked the possible benefit on the autocalibration procedure of the usage of eq. 1 corrected by a factor 0.75 to take into account the observed $(\frac{T}{T_0})_{fitted}$ vs $(\frac{T}{T_0})_{measured}$ slope. An rt relation measured at a temperature T_0 was thus used to produce a new rt by applying eq. 1

with a correction factor 0.75 and $\Delta T = 3.4\ K$. This was used as the starting rt in the iterative procedure performed by CALIB on a data sample at an average temperature of $T_0 + \Delta T$. The residuals after the first iteration as a function of the drift time, prior to any correction, are shown in fig. 21: at this level, the residual is just the difference between the starting rt and the track fit performed on the data sample using this rt relation. The result is very satisfactory, residual effect being confined at the 2-3 μm level and showing that the procedure is self-consistent.

7 Conclusions

Temperature and gas composition effects on drift time spectra and rt relations of MDT BIL chambers of Atlas have been studied with the cosmic ray Roma Tre test stand.

Temperature effects on the maximum drift time length have been measured to be $-2.34 \pm 0.06\ ns/K$ in good agreement with analogous results obtained at the H8 test beam setup and in marginal agreement with the expectations of the Garfield simulation program.

Effects on rt relations due to changes in gas composition have been measured to be large: differences of about 200 μm for large drift times have been observed for a gas composition change of 0.3% absolute in CO_2.

Temperature effects on rt relations have been precisely measured and found to be linear and in good agreement with Garfield expectations at 15 μm level. It was found that a simple analytical parametrisation, slightly modified with respect to the original proposal [1] for the presence of an overall correction factor, can be used to describe quite accurately the observed temperature effects. Its use in the autocalibration procedure is self-consistent to the level of very few μm.

The studies of temperature effects on rt relations allowed to access the size of some systematics of the autocalibration procedure at levels below 10 μm and below 0.3 ns in space and time respectively. Such studies could become a benchmark for the comparison of different autocalibration methods.

8 Acknowledgements

We thank warmly R. Lomoro, S. Loffredo and F. Budano for their technical assistance on the temperature probe system.

References

[1] M.Aleska,W.Riegler: Non-Linear MDT Drift Gases like Ar/CO_2. Atlas Internal Note December 1998

[2] ATL-MUON-2003-008. BIL Chamber Tests in Roma Tre ATL-MUON-2001-007. The cosmic ray hodoscope for the MDT chamber test site in Roma Tre.

[3] com-muon 2002-004 CALIB: A package for MDT calibration studies. User Manual.

[4] ATL-MUON-2003-001. Atlas Internal Note 20 October 2001.

[5] R.Veenhof, GARFIELD : a drift chamber simulation program, CERN program library W5050.